

A Parylene Neural Probe Array for Multi-Region Deep Brain Recordings

Xuechun Wang[✉], Student Member, IEEE, Ahuva Weltman Hirschberg, Huijing Xu, Member, IEEE,

Zachary Slingsby-Smith, Aziliz Lecomte, Kee Scholten[✉], Member, IEEE,

Dong Song[✉], Senior Member, IEEE, and Ellis Meng[✉], Fellow, IEEE

Abstract—A Parylene C polymer neural probe array with 64 electrodes purposefully positioned across 8 individual shanks to anatomically match specific regions of the hippocampus was designed, fabricated, characterized, and implemented *in vivo* for enabling recording in deep brain regions in freely moving rats. Thin film polymer arrays were fabricated using surface micromachining techniques and mechanically braced to prevent buckling during surgical implantation. Importantly, the mechanical bracing technique developed in this work involves a novel biodegradable polymer brace that temporarily reduces shank length and consequently, increases its stiffness during implantation, therefore enabling access to deeper brain regions while preserving a low original cross-sectional area of the shanks. The resulting mechanical properties of braced shanks were evaluated at the benchtop. Arrays were then implemented *in vivo* in freely moving rats, achieving both acute and chronic recordings from the pyramidal cells in the cornu ammonis (CA) 1 and CA3 regions of the hippocampus which are responsible for memory encoding. This work demonstrated the potential for minimally invasive polymer-based neural probe arrays for multi-region recording in deep brain structures. [2020-0018]

Index Terms—Brain-computer interfaces, chronic recording, flexible brain probe, multielectrode array, Parylene C.

I. INTRODUCTION

FUNDAMENTAL neuroscience research and neuroprosthetic technologies require neural interfaces capable of high-resolution electrophysiological recording and stable, long-term performance. Penetrating microelectrode arrays produced using conventional silicon micromachining techniques

Manuscript received February 5, 2020; revised May 2, 2020; accepted May 22, 2020. Date of publication June 22, 2020; date of current version July 31, 2020. This work was supported in part by the NSF INSPIRE under Grant CBET-134193 and in part by the NIH BRAIN under Grant U01 NS099703. Subject Editor K. Cheung. (*Corresponding author: Ellis Meng*)

Xuechun Wang, Huijing Xu, Kee Scholten, and Dong Song are with the Biomedical Engineering Department, University of Southern California, Los Angeles, CA 90089 USA (e-mail: xuechunw@usc.edu; huijingx@usc.edu; kscolte@usc.edu; dsong@usc.edu).

Ahuva Weltman Hirschberg is with the Keck School of Medicine, University of Southern California, Los Angeles, CA 90033 USA (e-mail: aweltman1@gmail.com).

Zachary Slingsby-Smith is with the Electrical Engineering Department, Imperial College London, London SW7 2BU, U.K.(e-mail: zsmith@usc.edu).

Aziliz Lecomte is with the Fondazione Istituto Italiano di Tecnologia, 16163 Genova, Italy (e-mail: aziliz.lecomte@gmail.com).

Ellis Meng is with the Biomedical Engineering and Electrical and Computer Engineering Department, University of Southern California, Los Angeles, CA 90089 USA (e-mail: ellis.meng@usc.edu).

Color versions of one or more of the figures in this article are available online at <http://ieeexplore.ieee.org>.

Digital Object Identifier 10.1109/JMEMS.2020.3000235

common to microelectromechanical systems (MEMS) can support 10's to 100's of recording sites on shanks having widths of \sim 100 microns and measuring several millimeters in length; recent efforts are approaching 1000's of sites [1]–[3]. These tools offer high spatiotemporal resolution neural recording, but often fail under chronic *in vivo* conditions. One culprit is the mechanical stiffness of the silicon probes [4]; the mismatch in stiffness of common MEMS materials ($E \sim 150$ GPa [5]) and brain tissue (~ 6 kPa [6]) has been identified as a potential cause of chronic injury to the brain and associated retaliatory immune response [7]–[9]. Instability at the device-tissue interface arising from micromotion can result in neuronal death and glial scarring in the surrounding tissue which prevents acquisition of neural recordings beyond weeks or months after implantation [4], [7], [10]–[12].

To improve the recording lifetime of these devices, penetrating microelectrode arrays made from softer materials in a variety of different form factors are being explored as a mean to minimize the chronic foreign body response [8], [13], [14]. These materials include polyimide [15]–[17], SU-8 [18]–[21], poly-(para-chloro-xylylene) (Parylene C) [22]–[24], thermoset shape memory polymer (SMP) such as thiol-ene/acrylate [25]–[27], composite material containing elastomers such as polydimethylsiloxane (PDMS) [28], [29], and soft-nanocomposites made from cellulose fiber scaffold [14], [30], [31]. The consequence of using low elastic moduli materials is that the long, slender neural probe shanks are susceptible to mechanical buckling during insertion into brain tissue [32], [33] which prevents accurate targeting and access to deep brain structures. In practice, penetrating polymer microelectrode arrays are limited to superficial brain targets (< 3 mm deep).

In order to access and study deeper brain structures such as the hippocampus, thalamus, and basal ganglia across species with brains of varying sizes [34]–[36], there is a need for longer penetrating polymer probes that overcome these surgical placement challenges. A common approach is to temporarily stiffen the probe shank to avoid buckling. Examples include insertion shuttles [22], [37]–[42] which are temporarily coupled to the probe and then retracted following implantation, and water-soluble coatings such as silk [43], [44], polyethylene glycol (PEG) [45]–[47], tyrosine-derived polymers [48], [49], gelatin [50], [51], saccharose [52], [53], maltose [54], and carboxy- methylcellulose (CMC) [55] coated over the probes, which increases the effective Young's modulus of the

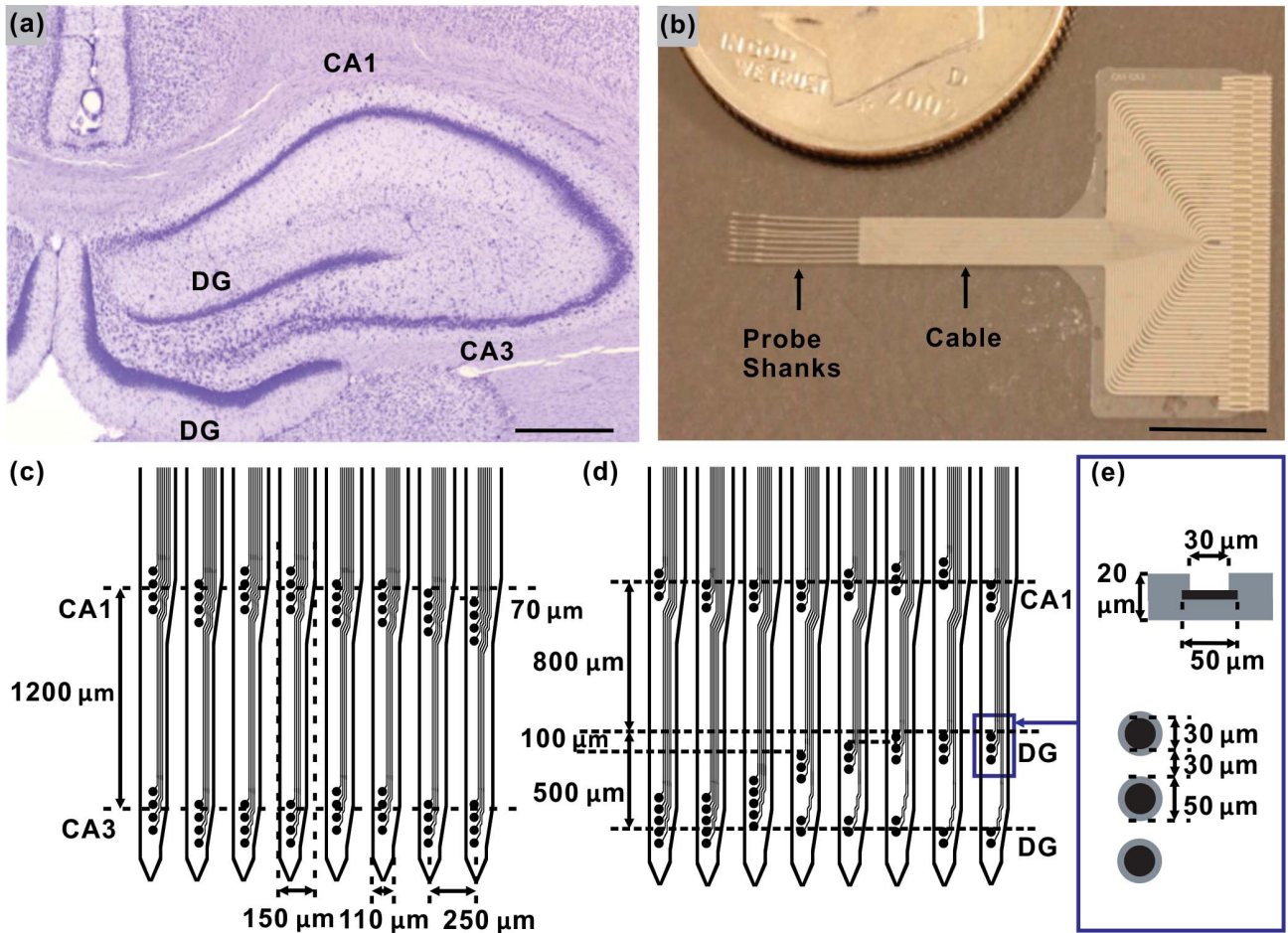


Fig. 1. (a) Cresyl violet stained coronal rat hippocampus slice showing the location of sub-regions CA1, CA3 and DG (dentate gyrus, scale bar = 600 μm). (b) Fabricated brain probe array compared to US dime (scale bar = 5 mm). (c) Schematic showing probe design with electrode layout to target CA1 and CA3 regions. (d) Schematic showing probe design with electrode layout to target CA1 and DG. (e) As-fabricated electrodes are 50 μm in diameter of which 30 μm is exposed after applying surrounding insulation. The center-to-center distance between the electrodes is 70 μm . Probe arrays measured 20 μm in thickness and consisted of a Parylene C-platinum-Parylene C sandwich.

assembly. However, these approaches significantly increase the cross-sectional area of the probe shank. This in turn increases acute injury to the brain which further contributes to an increase in gliosis and isolation of recording sites [56]. The impact of introducing a high concentration of coating material at the tissue-device interface on neuronal health, recording quality, and local brain chemistry is not known and requires further investigation.

Few polymer penetrating neural probes targeting the hippocampus in rat (> 3 mm deep) were reported; these devices possessed a single probe shank with regularly spaced electrode layouts that do not conform to the anatomy of hippocampal circuits [27], [57]. To address the need for high channel count probe arrays that can access multiple regions of the hippocampus, we introduced a novel method for deep brain implantation of micromachined Parylene C-based probe arrays that preserved the original as-fabricated shank cross-section to minimize acute insertion trauma [58], [59]. The back end of probes was braced in a dissolvable polyethylene glycol (PEG) slab to temporarily shorten the probe length and increases its stiffness during initial implantation [60]. The 64-site recording array

had 5.5 mm long shanks that reached structures as deep as 4.5 mm, electrode sites positioned to match the laminar anatomy of the hippocampus, and a layout targeting multiple regions simultaneously (Fig. 1). We reported preliminary results demonstrating the deep brain insertion concept and acute *in vivo* recordings in rat [24], [58]. The present work details the array design, microfabrication, mechanical characterization of the array for the implantation technique involving a biodegradable polymer brace, electrochemical characterization of microelectrode sites using cyclic voltammetry (CV) and electrochemical impedance spectroscopy (EIS), packaging method, and *in vivo* results supporting the potential for long-term use of these arrays.

II. PROBE ARRAY DESIGN

The neural interface of the hippocampal array was designed to span a 2000 μm length of brain along the septal-temporal axis with eight probe shanks that are separated by 250 μm center-to-center (Figs. 1 and 2). Each shank was constructed using a 20 μm thick Parylene C-platinum-Parylene C

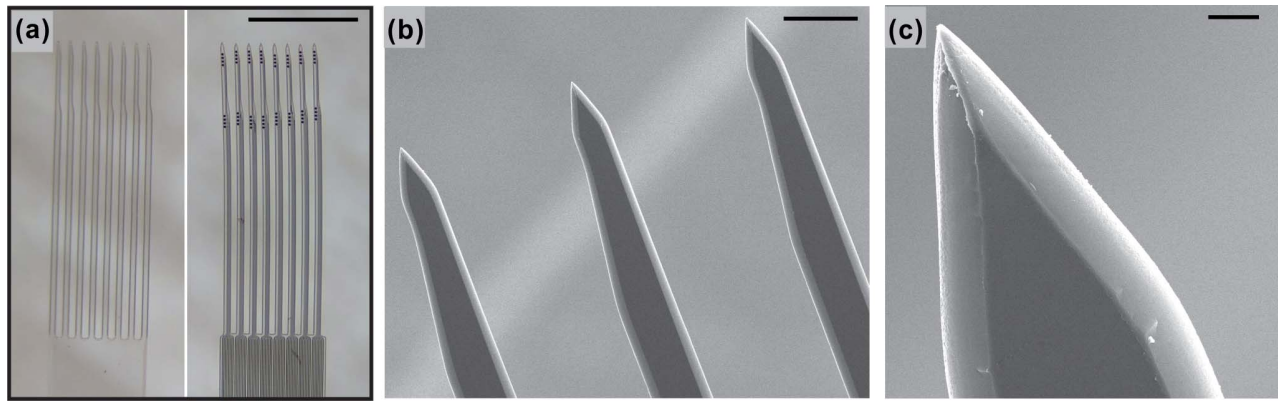


Fig. 2. (a) Optical micrographs showing shank array for a sham Parylene device (left) and a completed Parylene device with electrodes (right). Scale bar = 2 mm. (b) SEM micrographs showing the tip region of the array (scale bar = 100 μm) and (c) a single probe tip (scale bar = 10 μm).

sandwich measured 5.5 mm in length, and terminated in a pointed tip with a 45° angle. Numerous studies describe the fabrication and *in vivo* performance of both rigid and soft neural probes having different designs including tip geometries and probe dimensions [5], [61]–[65]. The array geometry and dimensions were chosen in the range reported in literature corresponding to relatively less tissue damage [10], [11]. The width of an individual shank expanded from the pointed tip to 110 μm and then slightly widened to a maximum of 150 μm . Each shank had 8 electrodes for a total of 64 electrodes across the 8-shank array. On each shank, the 8 electrodes were arranged in two or three linear clusters in order to match the geometry of the rat hippocampus and specifically place electrodes in the CA1-CA3 or CA1-DG regions. Thus, in total, two different arrays were designed to target specific regions in the trisynaptic circuit of the hippocampus (Fig. 1).

To surgically insert these soft polymer probes, their mechanical performance must be considered. A single neural probe can be modeled as a thin, uniform beam, with one end fixed and the other end pinned against the brain's surface at the moment of implantation. Euler's buckling formula (Eq. 1), approximates the force required to buckle a probe of length L , width w , thickness t , Young's modulus E , and an effective length factor k [15], [54], [61], [66], [67].

$$F_{\text{Euler}} = \frac{\pi^2 E w t^3}{12 (kL)^2} \quad (1)$$

The column effective length factor, k , captures the degree to which each end of the column is constrained against movement. During insertion into brain tissue, the base of the probe is considered to be clamped to the insertion tool and fixed (allowing for no translation or rotation), and the tip of the probe is free to move laterally as soon as it contacts brain tissue where k is 2. As the tip moves and further deforms the brain surface without penetration, the boundary condition changes to be pinned in the x-y plane (only allows for rotation, not translation). Accordingly, the commonly accepted value of k is 0.7, validated experimentally in [32]. Once the probe has penetrated the tissue, however, both ends of the probe are now effectively fixed and k drops to 0.5, yielding a higher buckling force threshold. This predicts that probes inserted in tissue can

withstand more stress without buckling when inserting deeper into the brain according to (1).

However, (1) also indicates that polymer probes having low Young's modulus and long shanks have low buckling force. Insertion shuttles and over-coatings can increase the buckling force to exceed the force required to penetrate brain tissue. Alternatively, it is possible to increase buckling force by decreasing length (L). In order to reach deep brain structures beyond the first few millimeters, this decrease in length needs to be temporary. This motivates the approach here to use a dissolvable brace that temporarily shortens probe length and increases buckling force during implantation. Removal of the brace returns probes back to their native mechanical properties.

III. FABRICATION AND PACKAGING

A. Fabrication of Probe Arrays

All polymer devices are micromachined in a layer-by-layer process on a bare 4" silicon (Si) wafer. The wafer was pre-baked at 110 °C (> 10 mins) prior to fabrication to dehydrate the surface. A base layer of 10 μm thick Parylene C (Specialty Coating Systems, Indianapolis, IN) was deposited by chemical vapor deposition (CVD) under vacuum. A 1.5 μm thick AZ5214-IR (Integrated Micro Materials, Argyle, TX) layer was spin coated on top of the base Parylene C layer (step 1: 8 s, 500 rpm, step 2: 45 s, 2,000 rpm) and then patterned via photolithography as a liftoff mask used to define the electrode sites (50 μm diameter) and metal traces (5 μm width with 5 μm spacing). Before platinum deposition, the wafer surface was cleaned and the Parylene C activated using O₂ plasma in a reactive ion etcher (RIE) (Technics, 800 Series Micro RIE System) at 100 W and 100 mTorr for 1 minute. 2000 Å of platinum was deposited by electron-beam deposition (Caltech Kavli Nanoscience Institute, Pasadena, CA). Excess metal was lifted off in acetone heated to 50 °C with gentle brushing to dislodge excess metal between the traces and followed by successive rinses in isopropyl alcohol (IPA) and deionized (DI) water for 5 minutes. Prior to the deposition of a second Parylene C layer, wafers were cleaned, and the Parylene C was activated in O₂ plasma at 100 W and 100 mTorr for 1 minute

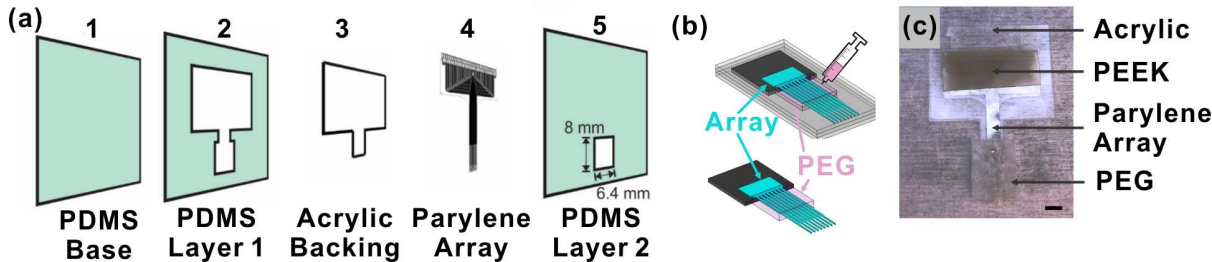


Fig. 3. Fabrication process for the PEG brace. (a) An exploded view of the mold parts is depicted and followed by (b) the assembled mold and method of PEG brace application. (c) Parylene C array with PEG brace after releasing from the mold (scale bar = 2 mm).

and then dehydrated at 110 °C under vacuum (> 10 mins). A second 10 μm thick Parylene C insulation layer was deposited. AZ4620 (Integrated Micro Materials, Argyle, TX) was spin coated (step 1: 5 s, 500 rpm, step 2: 45 s, 1200 rpm) to form a 15 μm thick etch mask that defined the device and probe outline. The device outline was then etched 10 μm deep using a switched chemistry process in a deep reactive ion etcher (DRIE, Oxford Plasma Lab System 100; 700 W ICP, 80 W RF power, 23 mTorr) [68]. The remaining photoresist mask was removed in acetone, IPA, and DI water. A subsequent 30 μm thick AZ4620 mask (two spins separated by softbake at 90 °C for 12 minutes, both spins performed in two steps with step 1: 8 s, 500 rpm and step 2: 45 s, 2000 rpm) was used as a mask for the final switched chemistry $\text{C}_4\text{F}_8/\text{O}_2$ etch step (same parameters as above) which exposed electrodes and contact pads and completed the array outline. The electrode sites and contact pads were etched out at the end of the process to avoid scum deposition from another micromachining process. The remaining photoresist was stripped by rinsing in acetone, IPA, and DI water. To release devices from the wafer, devices were soaked in DI water and gently peeled away from the native oxide layer on the silicon substrate. Released Parylene C arrays were annealed to increase Parylene C chain entanglement and reduce stress [69]. For this process, arrays were sandwiched between two Teflon sheets lining two glass slides and the assembly was held together with clips. Arrays were placed in an oven, vacuum purged three times with N_2 , and then annealed under vacuum for 48 hours at 200 °C [70]. The intermediate Teflon layer prevented Parylene C from irreversibly adhering to the glass slides.

B. Fabrication of Mechanical Shams

In order to develop the surgical insertion method, probe arrays having identical geometry and dimensions but without any metal features were prepared (Fig. 2a). A 20 μm thick layer of Parylene C was deposited on a 4" dehydrated prime silicon wafer via two consecutive depositions of 10 μm each. AZ 4620 photoresist was spin coated to serve as an etch mask (30 μm thick) and patterned via photolithography to define the probe array outline. Parylene C was etched via switched chemistry $\text{C}_4\text{F}_8/\text{O}_2$ DRIE (~ 230 loops, 700 W ICP, 20 W RF Power, 23 mTorr). The photoresist mask was then stripped in sequential baths of acetone, IPA, and DI water. Devices were individually released by gently peeling under DI water immersion.

C. Molding of PEG Brace

Arrays were temporarily stiffened for insertion into the brain by applying a slab of water-soluble polyethylene glycol (PEG) to the base of the shanks, forming a mechanical brace and shortening the effective exposed shank length from 5.5 to 1 or 2.8 mm for *in vivo* and *in vitro* benchtop testing, respectively. According to (1) ($k = 0.7$, $E = 2.76 \text{ GPa}$ [71], 20 μm thick and 110 μm wide probe shank), a Parylene C probe with an effective length of ~ 2.8 mm can theoretically withstand $> 0.5 - 1.0 \text{ mN}$ of force without buckling, the commonly reported insertion force for penetrating the cortical tissue without dura mater [61], [62], [72]. For *in vitro* tests, probes were inserted into a flat agarose (Sigma-Aldrich, Darmstadt, Germany) mold as a representative mechanical brain phantom. For *in vivo* insertions, however, the brain surface is uneven which may cause the probe tips in an array to contact the brain at different time and increase the chance of buckling. Therefore, *in vivo* experiments were performed using only 1 mm of exposed shank length instead of 2.5 mm. This reduced length theoretically increased buckling force 6-fold according to (1).

PEG was selected as the dissolvable material for its availability in a range of molecular weights (MW) which allows the dissolution rate to be tuned. In addition, it is easy to prepare and apply and has anti-immunogenic and antigenic properties [73]. The process to apply the PEG brace onto the array is depicted in Fig. 3 [24]. Molten PEG (Sigma-Aldrich, Darmstadt, Germany; MW 3350) was injected into a three-layer polydimethylsiloxane (PDMS, McMaster-Carr, Elmhurst, IL) mold that supported the array while the brace was applied in a 60 °C oven. A 0.5 mm thick acrylic backing was temporally attached to the cable portion of the probe (shown in Fig. 1b) through a PEG block. PDMS Layer 1 (0.5 mm, labeled 2 in Fig. 3) contained a pocket defined by a vinyl cutter (Graphtec® cutting plotter CE6000-40, Irvine, CA) as a receptacle to receive the acrylic backing and define the brace. The top PDMS layer (0.5 mm thick) also contained a precisely cut slot and was used to complete the top half of the brace. After filling, the entire assembly was cooled down to room temperature to allow the PEG to solidify. The braced array was released by carefully peeling away the mold starting from the contact pad end to the probe tips.

D. Electrical Packaging

The implanted neural interface incorporated a flexible ribbon cable (5 μm wide platinum traces with 5 μm edge-to-edge spacing) that fanned out and terminated in a contact pad array.

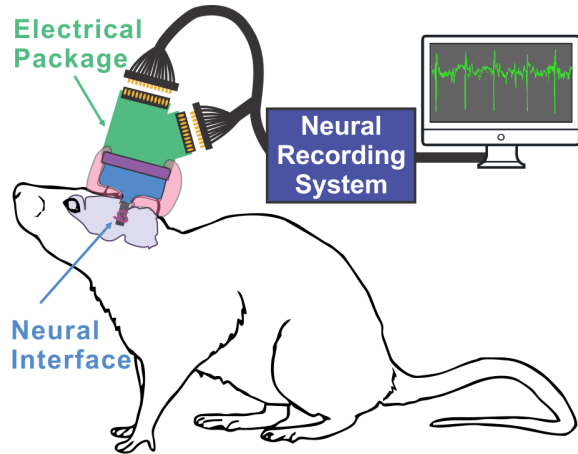


Fig. 4. Illustration of the implanted array, electrical packaging, and recording setup for the *in vivo* study.

The back side of this portion was supported by a 0.05 mm thick polyether ether ketone (PEEK) tape with a 0.06 mm thick acrylic adhesive (CS Hyde Co., Lake Villa, IL) (Fig. 3c) to build up the thickness of the probe for mating to a 71 pin zero insertion force (ZIF) connector (Hirose Electric Co., Japan). This ZIF connector bridged the recording electrodes via a printed circuit board (PCB; Gold Phoenix PCB, China) to two Omnetics connectors (Omnetics Connector Corporation, Minneapolis, MN) for direct connection to the electrophysiological recording system (Fig. 4). The acrylic backing attached to the probe was then matched to the ZIF height and attached to the backside of PCB through a double-side tape (Fig. 5c).

Two PCB designs were developed; the first was previously described but abandoned due to excessive height [24]. The first version utilized an SSB6 PCB to PCB connector (Molex Incorporated, Lisle, IL) to allow repeated use of costly Omnetics connectors (Fig. 5a, left and 5b, top). However, the SSB6 connector could not support frequent connections and disconnections. As the connectors had limited lifetime, the scheme was only used in the first animal. To reduce the size of the head-mounted electrical packaging, a single-PCB approach was developed that directly adapted the two connector types and angled one Omnetics connector at $\sim 70^\circ$ from the horizontal to minimize overall PCB size (Fig. 5a, right and 5b, bottom). Built-in ground traces were added to decrease external sources of noise from movement of the ground wires (Fig. 5c).

IV. EXPERIMENTAL METHODS

A. PEG Dissolution Study

The dissolution rate of the brace must allow sufficient time for surgical handling and insertion while not dramatically extending the duration of surgery. To determine the appropriate molecular weight that balances these requirements, a dissolution experiment was performed using PEG discs ($N = 3$) having varying MW (1000, 3350, 8000 and 14,000 Da). PEG was melted in an oven heated to 60 °C and mixed with blue food dye. Molten PEG discs were injected into circular

molds (5 mm diameter in 1 mm thick PDMS sheet; Sylgard 184, Dow Corning Corp., Midland, MI). Excess PEG was removed from the top of the mold and after cooling, the PDMS mold was peeled away (Fig. 6). Discs were placed in plastic boxes (VWR International, Brisbane, CA) and fully submerged in 3 mL of 1X phosphate buffered saline (PBS, EMD Chemicals, Darmstadt, Germany). Photographs were taken every 30 seconds for 6.5 minutes and analyzed using ImageJ to calculate % of the surface area of the PEG disc remaining.

B. Mechanical Evaluation of Probes

We measured the insertion and buckling forces for Parylene C probe arrays having different shank numbers (1, 2, 4, 6 or 8; $N = 5$ for insertion test; $N = 3$ for buckling test). Insertion force was measured only for shorter probes as it is not dependent on length. The shorter probes were obtained by covering half of the shank with PEG leaving 2.8 mm exposed. Differing shank numbers were obtained by cutting off unwanted shanks. A Bose model 3100 motorized bench coupled with a 50 g Honeywell load cell (Sensotec, Model 31, Columbus, OH) (Fig. 7a) was used to measure the insertion force. Probes were mounted on the Bose motorized clamp and driven vertically into a brain phantom (0.6% agarose) on the load cell at a constant speed of 0.01 mm/s to determine insertion force (Fig. 7b). The brain phantom composition was selected for its similarity to the bulk mechanical properties of brain tissue [74]. The insertion speed 0.01 mm/s was selected to minimize the shear force on the surrounding brain tissue, based on prior reports [75]. The agarose gel was prepared in transparent plastic boxes less than 48 hours before insertion trials and sealed in Parafilm to prevent water evaporation and maintain consistent properties across gel batches.

The force resolution of the Bose system, however, was inadequate to resolve single shank buckling force. Therefore, buckling force was obtained using an Instron 5940 Series Single Column Tabletop (Norwood, MA) for the different probe lengths (2.8 or 5.5 mm, Fig. 7c).

With a setup similar to that shown in Fig. 7a, the probe was driven against a metal plate at 0.01 mm/s. Force was recorded as a function of stage displacement. Data was analyzed in Origin software using the adjacent averaging filter.

C. Evaluation of Electrode Sites

Before applying the PEG brace in preparation for implantation, all 64 electrodes in each array were electrochemically evaluated using cyclic voltammetry (CV) and electrochemical impedance spectroscopy (EIS) using a 3-electrode setup on a Reference 600 potentiostat (Gamry Instrument, Warminster, PA) [76], [77]. A 1 cm² platinum plate was used as the counter electrode and the reference electrode was Ag/AgCl (3M NaCl, BASI, MF-2052, West Lafayette, IN). The setup was contained in a Faraday cage to minimize external noise. CV was performed at room temperature in 0.05 M H₂SO₄ (30 cycles from -0.2 to 1.2 V versus Ag/AgCl (3M NaCl), scan rate of 250 mV/s) and in the process, provided electrochemical cleaning of electrode surfaces [76], [78]. EIS was performed

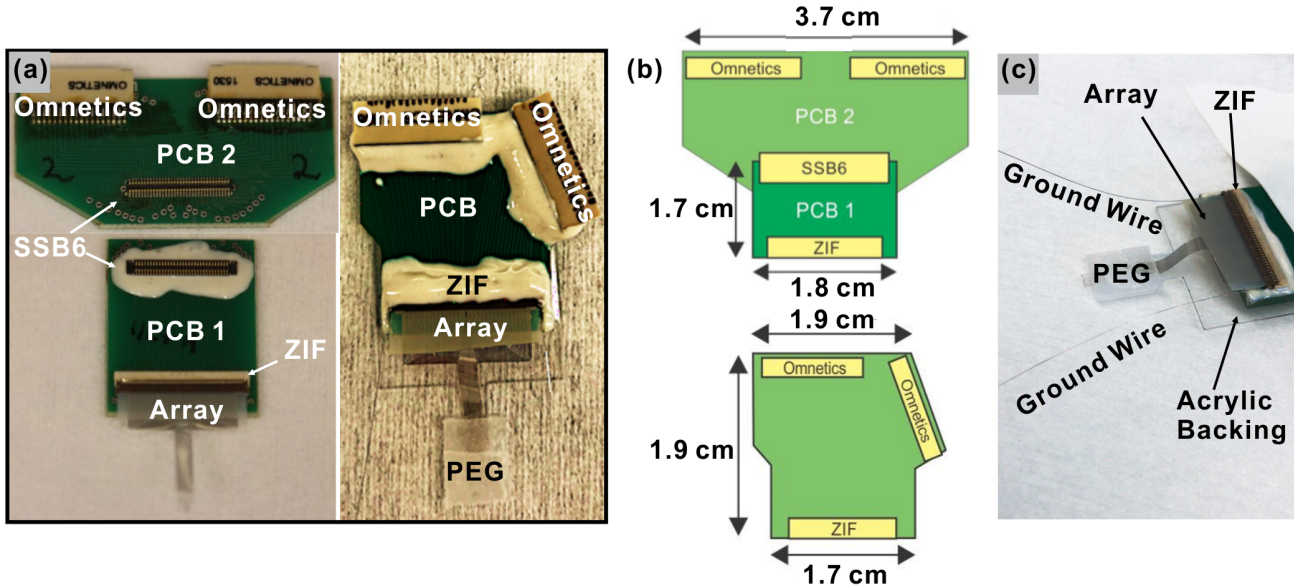


Fig. 5. (a) Fully packaged arrays using the original (left) and (right) revised PCB. (b) Comparison of the dimensions of the (top) original and (bottom) revised PCB designs. (c) A fully packaged array with the revised PCB shown in (a, right) and (b, bottom) highlighting the acrylic backing and the built-in ground wires.

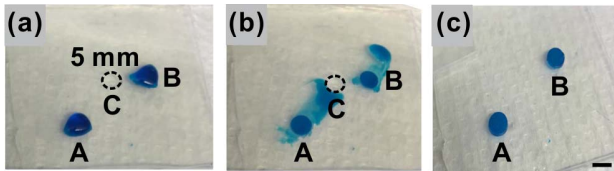


Fig. 6. The PDMS mold for PEG dissolution study. (a) PEG was heated to 60 °C to allow injection into a cylindrical well (diameter = 5 mm) in a PDMS mold. Wells A and B were filled with PEG mixed with blue dye and well C was empty (outline highlighted with black-dash circle). (b) Excess PEG was wiped away with a clean glass slide and the PEG allowed to cool in the mold to room temperature. (c) Molded PEG discs A and B were freed after peeling the top PDMS layer away. All scale bars are 5 mm.

in 1× PBS at room temperature (25 mV_{RMS}, 1–10⁶ Hz). Electrode impedance was analyzed at 1 kHz which is reported as the frequency where neurons fire action potentials [79]. Electrodes exhibiting at 1 kHz an impedance > 2 M Ω, or with uncharacteristic phase behavior, were considered as an open circuit and discarded during analysis.

D. In Vivo Demonstration in Rat Hippocampus

Probe arrays were implanted according to the guidance of both the Institutional Animal Care and Use Committee (IACUC) and the Department of Animal Resources of the University of Southern California (USC). The surgical procedure used [24] is summarized here.

Animals were anesthetized with isoflurane during the implantation surgery after a pre-implantation injection of ketamine and xylazine. A 2 × 4 mm cranial window was made above the hippocampus of a Sprague-Dawley rat and the dura was carefully removed with forceps. Five screws were anchored into the rat skull around the surgical window. The PCB was coupled to a stereotax with Parafilm for insertion.

The exposed probe tips of braced arrays were inserted into the brain until the PEG brace reached the surface of the brain. The brace was incrementally dissolved in saline and the newly exposed bare probe length was advanced in increments at a speed of 10 μm/s down to 4–5 mm depth (measured from probe tip contact with the brain surface, Fig. 8a). Dental cement was applied to the insertion site up to the PCB to secure the array (Fig. 8b). The animal was euthanized and perfused with paraformaldehyde after a few months of recording post implantation. After the array was removed from the brain, the brain tissue was dissected from the cranium, and the tissue was fixed in formalin overnight. The tissue was then dehydrated with 18% sucrose solution and sliced for histological staining.

During implantation of the array, neural signals from a single electrode were monitored with an oscilloscope to appropriately locate the target by recording of characteristic compound action potential recordings. For chronic recordings, each subject was given 7–16 days post implantation to recover, after which neural activities were recorded on a 64-channel data acquisition system (Plexon Inc., Dallas, TX) while the animal freely roamed at an open field. Simultaneous recordings from all 64 electrodes were captured at 40 kHz along with video recording (CinePlex, Plexon Inc., Dallas, TX) from the top of the open field to track the movement path of the animal [80]. Spike sorting (Offline Sorter, Plexon Inc., Dallas, TX) was applied to the recorded data offline.

V. EXPERIMENTAL RESULTS

A. PEG Dissolution Study

The dissolution rate (%/minute) across four different PEG formulations was obtained by dividing the dissolved area (%) in Table I by 6.5 minutes. While PEG 1000 dissolved at a rate of 9.5%/minute, PEG 3350 dissolved by a rate of 5.5%/minute.

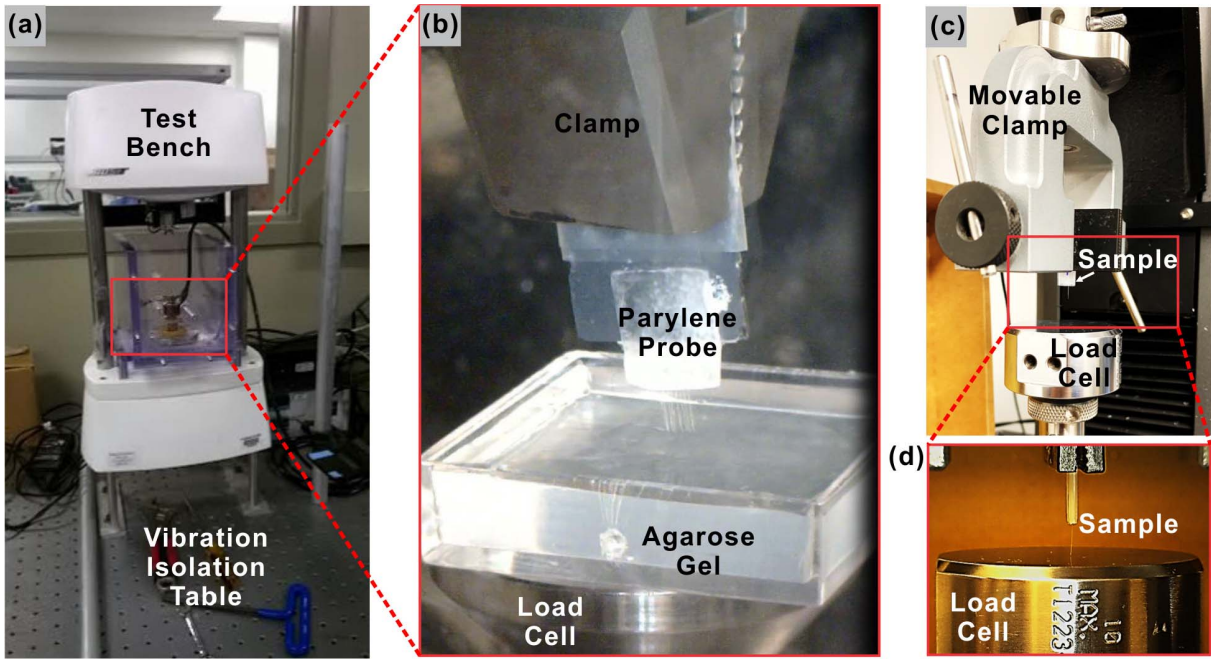


Fig. 7. (a) The mechanical testing setup for insertion force measurement. (b) Close-up view of the clamped probe array over an agarose gel block placed on the load cell. (c) The mechanical testing setup for buckling force measurement. (d) Close-up view of the clamped probe array over the Instron 5940 Series built-in load cell.

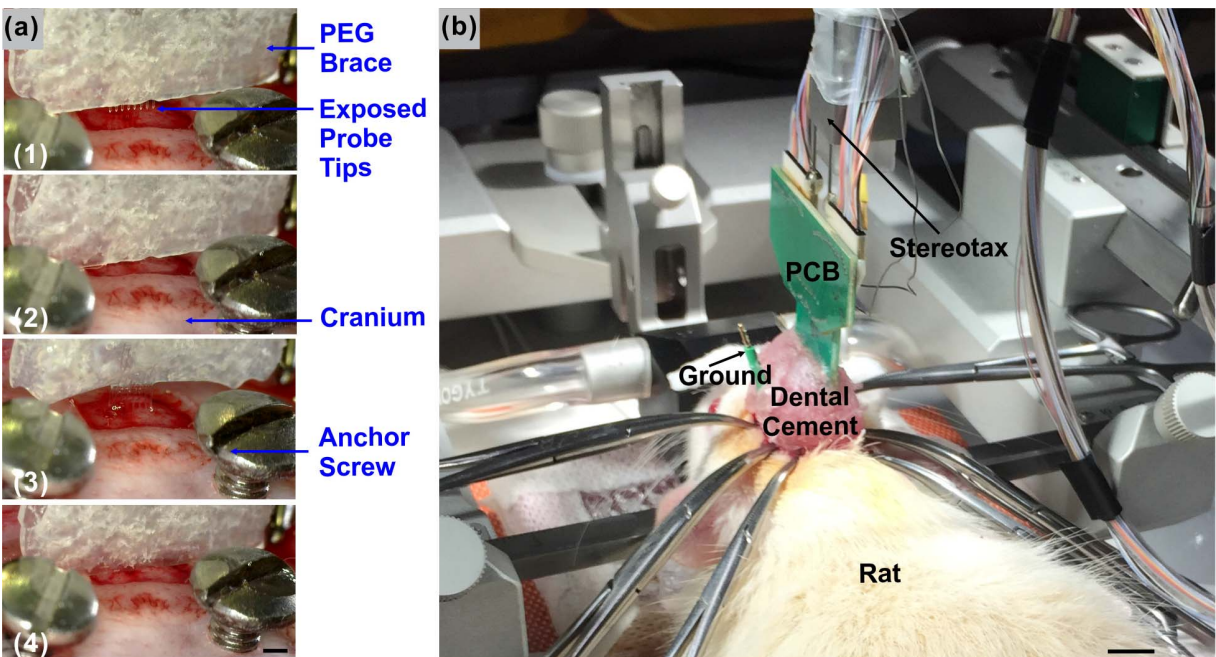


Fig. 8. (a) Insertion of Parylene C array supported with PEG brace into rat brain (scale bar is at 1 mm). (1) 1 mm of the probe shanks were exposed. (2) The exposed, bare shanks were inserted and advanced into the brain; (3) Saline dissolved away PEG to expose a portion of the shanks. (4) The newly exposed portion was advanced into the brain. This process can be repeated until the full length is inserted. (b) After insertion, the array is secured to the skull by using dental cement in preparation for recording (scale bar = 1 cm).

The dissolution rates of PEG 8000 and PEG 14000 (3.1 and 2.5%/minute, respectively) were too slow to be practical in a surgical setting. Since the PEG must withstand transport and not be susceptible to mechanical deformation from small amounts of water absorption, PEG 3350 was selected for further experiments and surgical insertion.

B. Mechanical Evaluation of Probes

Fig. 9 shows a representative mechanical measurement of the buckling force of a Parylene C probe array. The buckling force threshold was defined as the applied force to the entire array when all shanks buckled. Fig. 10 shows representative results from insertion tests of Parylene C probes into

TABLE I
REMAINING AREA OF PEG DISC ACROSS DIFFERENT MOLECULAR WEIGHT AFTER SUBMERGING IN 1X PBS FOR 6.5 MINUTES ($N = 3$)

Molecular Weight	Remaining Area (%)
1000	38
3350	64
8000	80
14000	84

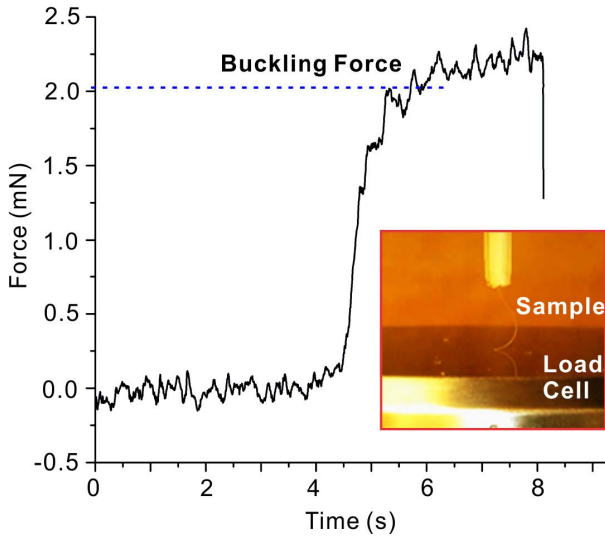


Fig. 9. A representative buckling force curve obtained with a 2.8 mm 8-shank Parylene C probe and smoothed with adjacent point average. The threshold force was taken with the setup in Fig. 7 (c). The buckling threshold force is highlighted with a blue dashed line. Inset shows the close-up view of a buckled 8-shank probe.

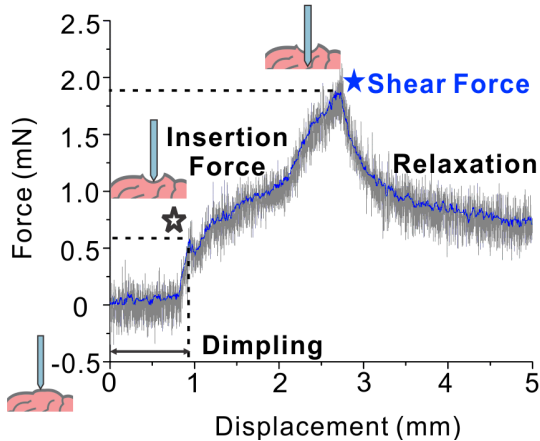


Fig. 10. A representative raw (grey) force-displacement data and smoothed curve (blue) with adjacent averages for a 2.8 mm 4-shank Parylene C probe during insertion into a block of 0.6% agarose gel. After the probe contacted the gel surface, the force increased until it reaches a threshold known as insertion force (labeled as a black unfilled star), which occurred when the probe initially penetrated the gel. Prior to that point, the probe displaced gel resulting in dimpling. As the probe advanced deeper, force increased until reaching the shear force (labeled as a blue solid star) at which point the maximum force was measured. This also corresponds to the completion of insertion. Then the probe rested in the gel corresponding to relaxation phase.

gel agarose. Insertion force was defined as the force required to initially pierce the brain phantom and the shear force as

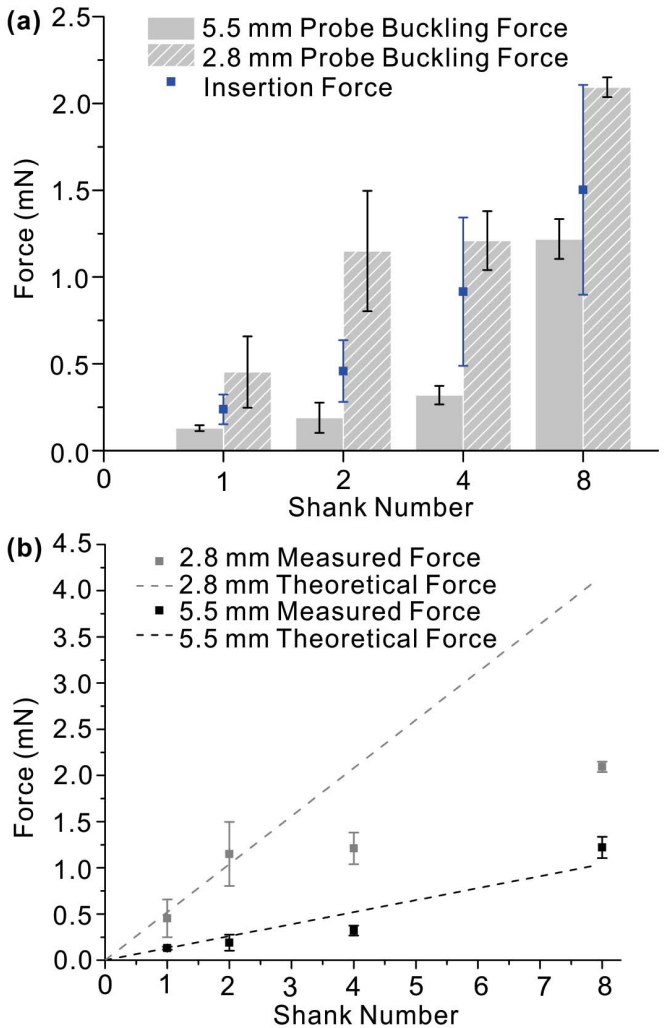


Fig. 11. (a) The buckling force thresholds (mean \pm SD, $N = 3$; bars) and insertion force (mean \pm SD, $N = 5$; blue squares). Buckling force is shown for 5.5 (solid) and 2.8 mm (hatched) shank lengths for single and multi-shank arrays (2, 4 and 8). (b) The buckling force as a function of shank number for both 2.8- (grey) and 5.5- mm (black) shank lengths (mean \pm SD, $N = 3$) was compared with the theoretical linear extrapolation calculated from (1).

the maximum force recorded as a function of the insertion depth [81].

The buckling force for probe arrays of up to 8 shanks, of full or shortened length, was compared to the measured insertion force in Fig. 11a. Notably in all cases, the 5.5 mm probes buckled at forces below that required for insertion, confirming prior observations that long, thin, polymer probes cannot be implanted into brain tissue successfully (Fig. 12). As expected, shorter probes had a higher threshold for buckling, but for larger arrays, the buckling force was within a standard deviation of the insertion force, prompting the need to shorten arrays even further for *in vivo* implantation as a measure of safety.

Fig. 11b compared the experimentally determined buckling force as a function of array size to the theoretical buckling force for a single probe as calculated with (1) ($k = 0.7$, $E = 2.76$ GPa, $w = 110 \mu\text{m}$, $t = 20 \mu\text{m}$). A single shank Parylene C probe ($L = 5.5 \text{ mm}$) is expected to buckle at

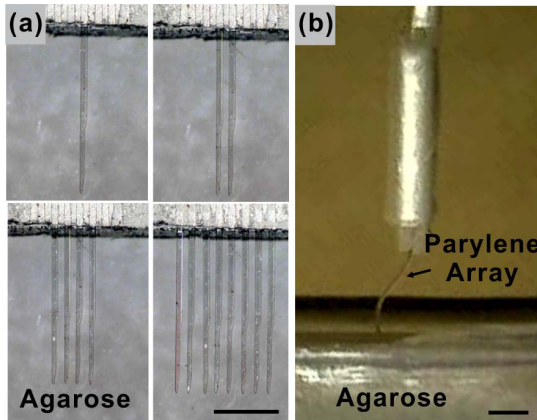


Fig. 12. (a) Braced Parylene C arrays (2.8 mm exposed) successfully inserted into the 0.6% agarose across all conditions (1, 2, 4 and 8 shanks; scale bar = 1 mm). (b) A single shank unbraced Parylene C probe (5.5 mm exposed) buckled before penetrating agarose (scale bar = 2 mm).

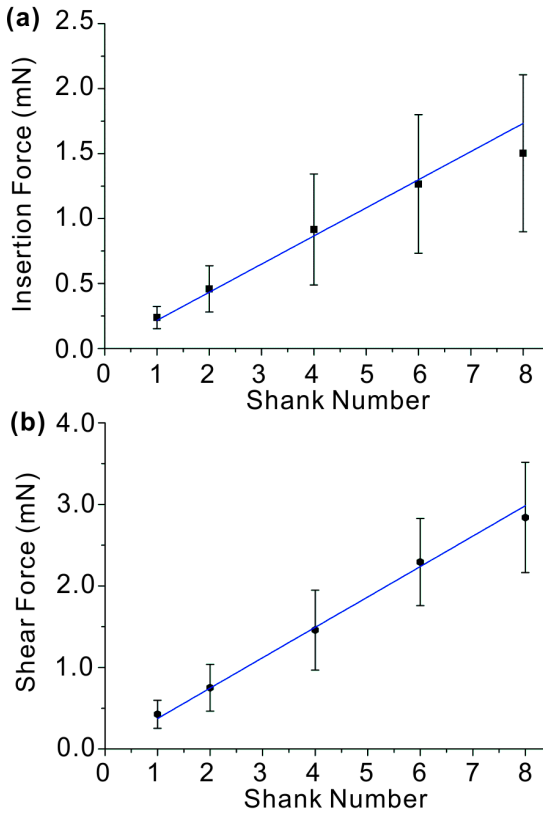


Fig. 13. Characteristic features of the force-displacement curve compared across different numbers of shanks: (a) insertion force, and (b) shear force (mean \pm SD, $N = 5$). Each plot exhibits a high degree of linearity as evidenced by the quality of the fit. Insertion force = $0.22 \times$ shank number, $R^2 = 0.99$; shear force = $0.37 \times$ shank number, $R^2 = 0.99$.

an applied axial force of 0.13 mN, and a shortened probe ($L = 2.8$ mm) at 0.52 mN. These calculations fall within the range of experimentally determined values: 0.13 ± 0.02 mN and 0.45 ± 0.21 mN, respectively. The buckling force for a Parylene C array probe did not scale linearly with shank number. The 8-shank array buckled at 1.22 ± 0.12 mN for the full length and 2.09 ± 0.06 mN at half length, a nine- and five-fold increase over single-shank measurements, respectively.

Fig. 13 shows the linear regression of insertion force and maximum shear force on arrays measured with 0.6% agarose

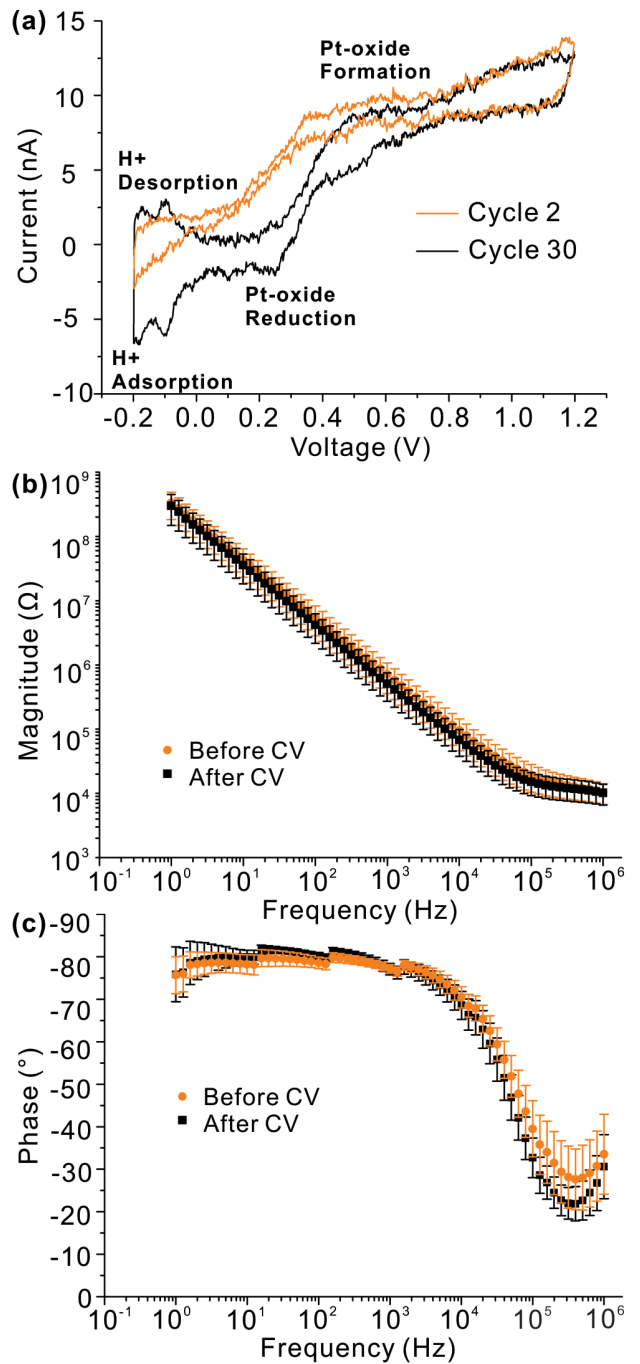


Fig. 14. (a) A representative CV curve of a single platinum electrode after 2nd cycle (orange) and 30th cycle cleaning (black) in the 0.05 M H₂SO₄. Characteristics peaks corresponding to oxidation-reduction reactions between platinum and the ions in the solution are labeled. (b) The electrochemical impedance spectroscopy (EIS) graph of the average electrode impedance magnitude (mean \pm SD, $N = 18$ electrodes) before (orange) and after (black) CV cleaning. (c) EIS phase curve taken before (orange) and after (black) CV cleaning (mean \pm SD, $N = 18$ electrodes). All electrodes are from a single device. The CV and EIS measurements were taken after the array was thermally annealed.

gel as a function of array size. For determination of shear force, all arrays were inserted to a depth of ~ 2.5 mm. The shear force for single shank was 0.43 ± 0.17 mN, comparable to values reported in the literature taken with the same insertion speed [75]. Both insertion and shear forces scaled linearly

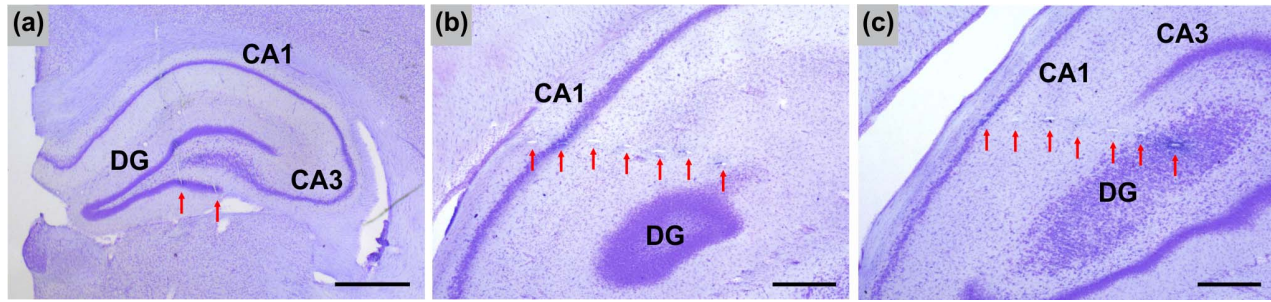


Fig. 15. Histological slices after Parylene C array implantation and removal highlighting the hippocampus. Slices were stained with hematoxylin and eosin. (a) Coronal and (b & c) transverse slices taken at 2.2 and 2.5 mm from the brain surface showing probe tracks (red arrows). Scale bar for (a) is at 1 mm; scale bar for (b & c) is at 500 μ m.

TABLE II
1 KHZ IMPEDANCE (MEAN \pm SD) OF DIFFERENT DEVICES

Device ID	Electrode Count	1 kHz Impedance ($k\Omega$)
A	53	734 \pm 238
B	63	795 \pm 364
C	62	718 \pm 147
D	59	695 \pm 122
E	60	883 \pm 141
F	61	556 \pm 132
G	62	468 \pm 279

with number of shanks ($R^2 > 0.99$, $N = 5$). As the number of shanks changed from 1 to 8, the insertion force increased six-fold (0.24 ± 0.09 mN changed to 1.50 ± 0.60 mN); the shear force increased seven-fold (0.43 ± 0.17 mN changed to 2.84 ± 0.68 mN).

C. Electrochemical Evaluation of Electrode Sites

Comparison of the CV curve taken after 2nd and 30th cycles suggests an increase in the electroactive area following the CV cleaning process (Fig. 14a). As the cycles progressed, the current response broadened at different voltages indicating increased cleanliness of the electrode surface area which allowed for more surface reactions and current flow. At cycle 30, the CV was comparable to a typical representative CV curve for Pt having characteristic peaks of Pt reaction in H₂SO₄ solution, indicating successful electrode cleaning. This improvement was also evident across the EIS data on electrodes obtained before and after the CV cleaning; impedance magnitude decreased slightly from 715 to 513 k Ω at 1 kHz (Fig. 14b). The mean impedance at 1 kHz across 7 different devices ($N = 420$ electrodes) was 691 ± 257 k Ω with variation between individual devices reported in Table II. After CV cleaning, the phase angle at higher frequency was more resistive (closer to 0°) and roughly constant at the lower frequency range (Fig. 14c).

D. In Vivo Evaluation

Surgical implantation lasted approximately 2 hours after alignment and included time for electrophysiological

monitoring of sites for characteristic compound spikes indicative of proper placement in hippocampus. Histological brain sections revealed that the stab wounds matched probe cross-sectional dimensions indicating minimal damage to surrounding tissues (Fig. 15). The spike amplitudes for units, noise levels for channels, and signal to noise ratios of recordings obtained by the Parylene hippocampal array under acute preparation were comparable to those of microwires (25 μ m diameter, stainless steel) [24]. The representative templates of spike waveforms of multiple units recorded from one animal are depicted in Fig. 16; 5 out 8 shanks recorded from both the CA1 and the CA3 region simultaneously, while the other three shanks recorded from either the CA1 or CA3 region due to the curved structure of the hippocampus. Over 80 neuronal units were recorded in this experiment. The results of long-term recordings are shown in Fig. 17a, with 3 out of 4 rats yielding recording with stable noise level over 5 weeks. Fig. 17b shows a representative recording through one channel from CA1 and CA3 region of an animal at 12 weeks. The maximum spike recorded had a signal amplitude of 330.10 μ V and a 3-sigma of noise level at 37.45 μ V. The probe with shanks able to capture signal from both CA1 and CA3 region was further used in the behavioral study with free-moving rat (Fig. 17c).

VI. DISCUSSION

Initial feasibility studies on mechanical insertion were performed using probe shams having no metal features. When adding the 2000 Å platinum conductor layer, curvature of the released probes was observed arising from intrinsic stress present in sputtered metal. This stress may have been exacerbated by the deposition process and its associated thermal transitions; the difference in thermal expansion coefficients between the metal and polymer films following temperature cycling during fabrication are also implicated [82]. Curvature in released probes is undesirable and inhibits precise insertion into the tissue along a straight path. Therefore, processes which result in high residual stresses in the metal film are undesirable. To eliminate curvature, the process was modified to utilize e-beam metal deposition (Fig. 18) in conjunction with post-fabrication controlled thermal annealing [70], [82].

Prior to developing the dissolvable brace, alternative insertion shuttles, including the use of lithographically defined

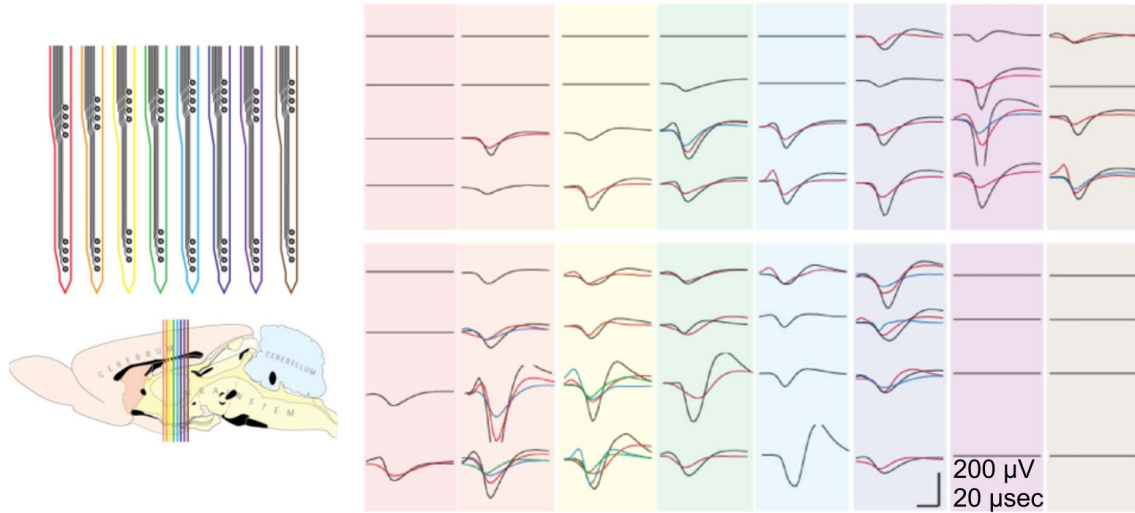


Fig. 16. Representative spike waveforms from multiple units recorded from one lightly anesthetized animal immediately after implantation.

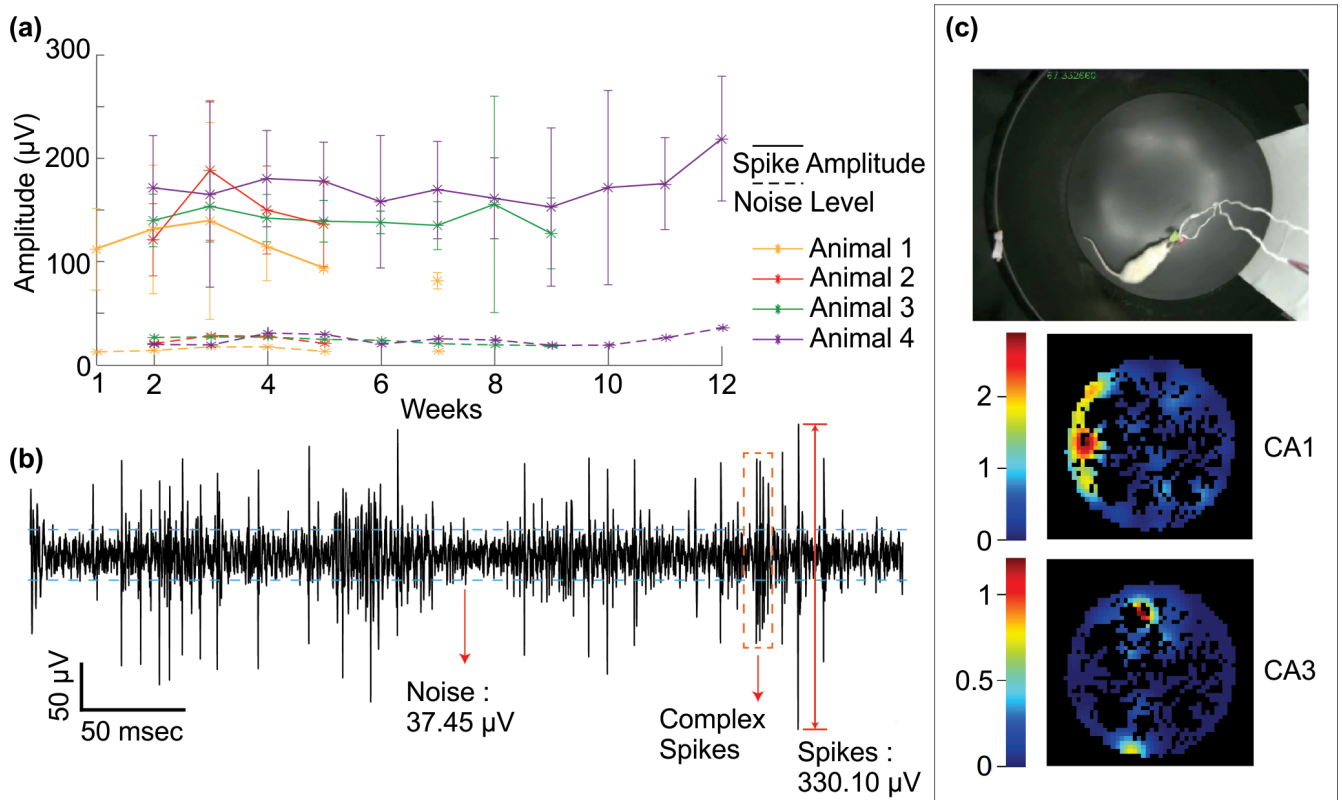


Fig. 17. Chronic recordings obtained with a Parylene C multi-electrodes array. (a) Average noise level (mean) and the spike amplitude (mean \pm SD) of neural signals recorded from four animals over 5 to 12 weeks post-implantation. (b) Representative recording from one animal at 12 weeks. The average spike amplitude of the units recorded from single neuron was $261.58 \mu\text{V}$ and the 3-sigma of noise level was $37.45 \mu\text{V}$. A group of complex spikes is identified in the orange dashed box. (c) The top shows the overhead frame capture of a rat running freely in an open field. The bottom two plots show the place field of two units simultaneously recorded at 12 weeks post-implantation from the CA1 and the CA3 sub-regions while the animal was running freely. The color bar represents the firing rate of neurons (in Hz).

'pockets' in conjunction with metal wires to place thin Parylene C shanks were evaluated. These approaches entailed increased the fabrication complexity and introduced new engineering challenges, and ultimately proved difficult to scale for larger arrays and smaller devices. In contrast, our dissolvable PEG brace approach proved reliable and robust. The approach

was simple to scale from one probe to an array of multiple shanks, and by tuning the exposed length, we could increase the buckling threshold as desired.

Measurements of buckling force suggest the force to buckle multi-probe arrays does not increase proportionally with the shank number. This is counterintuitive and suggests probe

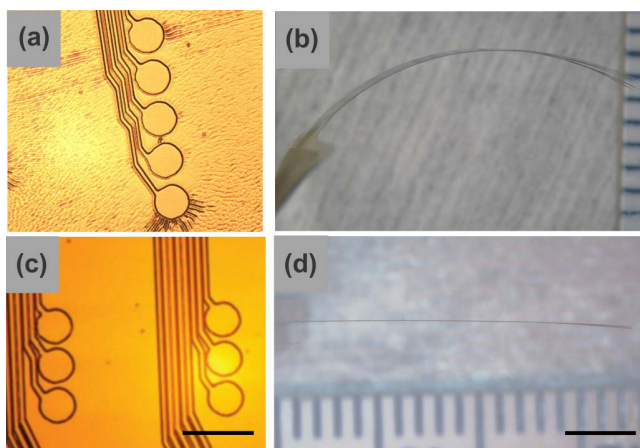


Fig. 18. High levels of compressive stress in sputtered platinum resulted in (a) ripples in the film and (b) severe probe curvature (viewed from side). E-beam deposited films, in contrast were (c) smooth and (d) no curvature was present. The scale bar for (a) and (c) is 100 μm ; the scale bar for (b) and (d) is 1 mm.

arrays cannot be modeled as a collection of independent beams. The discrepancy may result from differences in contact times between shanks and the metal plate, however such evidence was not apparent in our load cell or video recording data.

We observed greater shear force for arrays having more shanks while advancing into the brain after initial insertion; this relationship followed an approximately linear trend. A limitation of this study is that the shank-to-shank spacing is fixed and other spacing was not evaluated. Further study is also required to determine how these parameters scale as the arrays are expanded (e.g. by stacking linear arrays) to access three dimensions.

Insertion force measurements may be somewhat affected by the ability to align shanks parallel to the surface of the agarose gels (performed by eye). It is possible that, in some cases, shanks were misaligned and penetrated the agarose at different times. Slight inaccuracies in extrapolation of the insertion force from the experimental force curves may have resulted. When implanting in rat hippocampus, the brain surface is not flat however, this did not impact our ability to successfully insert the arrays. Overall, agarose gels are homogeneous and provide a simplistic mechanical model for rapid evaluation of insertion mechanics of soft polymer shanks prior to conducting *in vivo* studies. Successful insertion in agarose gels were reproduced *in vivo*. A limitation of the insertion experiments into agarose is that insertion force was acquired at one insertion speed. Shear force can be reduced at lower insertion speeds as this allows the tissue time to relax and accommodate the additional probe length more readily [75]. Simulations may be useful in deciding the proper spacing between shanks to allow for such relaxation.

VII. CONCLUSION

A flexible penetrating Parylene C-based neural probe array whose electrodes conform to hippocampal anatomy was designed, fabricated, characterized, and implemented *in vivo*.

In particular, the mechanical properties and performance of probe arrays were investigated, and the polymer material motivated the use of a novel bracing method to overcome premature mechanical buckling. Arrays were successfully implanted in agarose phantoms and rat brain using this bracing approach; bare shanks could be placed > 4 mm below the brain surface in a deep brain structure. The PEG brace was able to temporarily shorten the probe length to permit implantation and gain access to hippocampal structures. Simultaneous recordings from multiple electrode sites captured complex spikes which are characteristic of pyramidal cells in both the CA1 and CA3 regions of the hippocampus. Individual shanks inflicted minimal tissue disruption and left tracks within the tissue matching the bare probe cross-section.

The PEG bracing strategy overcomes challenges of minimally disruptive surgical implantation of soft polymer probes and can be generalized to other designs whether they are single or multi-shank. This technique is also likely generalizable to three dimensional multi-shanks arrays in addition to the linear arrays explored here.

ACKNOWLEDGMENT

The authors would like to thank Dr. Donghai Zhu, Kunhao Yu, Dr. Qiming Wang, and members of the USC Biomedical Microsystems Laboratory for their assistance.

REFERENCES

- [1] J. J. Jun *et al.*, "Fully integrated silicon probes for high-density recording of neural activity," *Nature*, vol. 551, no. 7679, pp. 232–236, 2017.
- [2] C. M. Lopez *et al.*, "A neural probe with up to 966 electrodes and up to 384 configurable channels in 0.13 μm SOI CMOS," *IEEE Trans. Biomed. Circuits Syst.*, vol. 11, no. 3, pp. 510–522, Jun. 2017.
- [3] P.-M. Wang *et al.*, "Challenges in the design of large-scale, high-density, wireless stimulation and recording interface," in *Interfacing Bioelectronics and Biomedical Sensing*. Cham, Switzerland: Springer, 2020, pp. 1–28.
- [4] R. Biran, D. C. Martin, and P. A. Tresco, "Neuronal cell loss accompanies the brain tissue response to chronically implanted silicon microelectrode arrays," *Exp. Neurol.*, vol. 195, no. 1, pp. 115–126, Sep. 2005.
- [5] K. Scholten and E. Meng, "Materials for microfabricated implantable devices: A review," *Lab Chip*, vol. 15, no. 22, pp. 4256–4272, 2015.
- [6] A. K. Ommaya, "Mechanical properties of tissues of the nervous system," *J. Biomech.*, vol. 1, no. 2, pp. 127–138, Jul. 1968.
- [7] T. D. Y. Kozai, A. S. Jaquins-Gerstl, A. L. Vazquez, A. C. Michael, and X. T. Cui, "Brain tissue responses to neural implants impact signal sensitivity and intervention strategies," *ACS Chem. Neurosci.*, vol. 6, no. 1, pp. 48–67, Jan. 2015.
- [8] J. Subbaroyan, D. C. Martin, and D. R. Kipke, "A finite-element model of the mechanical effects of implantable microelectrodes in the cerebral cortex," *J. Neural Eng.*, vol. 2, no. 4, pp. 103–113, Dec. 2005.
- [9] V. S. Polikov, P. A. Tresco, and W. M. Reichert, "Response of brain tissue to chronically implanted neural electrodes," *J. Neurosci. Methods*, vol. 148, no. 1, pp. 1–18, Oct. 2005.
- [10] T. D. Y. Kozai, A. L. Vazquez, C. L. Weaver, S.-G. Kim, and X. T. Cui, "*In vivo* two-photon microscopy reveals immediate microglial reaction to implantation of microelectrode through extension of processes," *J. Neural Eng.*, vol. 9, no. 6, Dec. 2012, Art. no. 066001.
- [11] R. Chen, A. Canales, and P. Anikeeva, "Neural recording and modulation technologies," *Nature Rev. Mater.*, vol. 2, no. 2, Feb. 2017, Art. no. 16093.
- [12] J. C. Williams, R. L. Rennaker, and D. R. Kipke, "Long-term neural recording characteristics of wire microelectrode arrays implanted in cerebral cortex," *Brain Res. Protocols*, vol. 4, no. 3, pp. 303–313, Dec. 1999.
- [13] A. Weltman, J. Yoo, and E. Meng, "Flexible, penetrating brain probes enabled by advances in polymer microfabrication," *Micromachines*, vol. 7, no. 10, p. 180, Oct. 2016.

- [14] J. K. Nguyen *et al.*, "Mechanically-compliant intracortical implants reduce the neuroinflammatory response," *J. Neural Eng.*, vol. 11, no. 5, Oct. 2014, Art. no. 056014.
- [15] P. J. Rousche, D. S. Pellinen, D. P. Pivin, J. C. Williams, R. J. Vetter, and D. R. Kipke, "Flexible polyimide-based intracortical electrode arrays with bioactive capability," *IEEE Trans. Biomed. Eng.*, vol. 48, no. 3, pp. 361–371, Mar. 2001.
- [16] J. E. Chung *et al.*, "High-density, long-lasting, and multi-region electrophysiological recordings using polymer electrode arrays," *Neuron*, vol. 101, no. 1, pp. 21–31, 2019.
- [17] R. Fáth *et al.*, "Long-term recording performance and biocompatibility of chronically implanted cylindrically-shaped, polymer-based neural interfaces," *Biomed. Eng./Biomedizinische Technik*, vol. 63, no. 3, pp. 301–315, Jun. 2018.
- [18] X. Wei *et al.*, "Nanofabricated ultraflexible electrode arrays for high-density intracortical recording," *Adv. Sci.*, vol. 5, no. 6, Jun. 2018, Art. no. 1700625.
- [19] A. Altuna *et al.*, "SU-8 based microprobes for simultaneous neural depth recording and drug delivery in the brain," *Lab Chip*, vol. 13, no. 7, pp. 1422–1430, 2013.
- [20] S.-H. Huang, S.-P. Lin, and J.-J.-J. Chen, "In vitro and in vivo characterization of SU-8 flexible neuroprobe: From mechanical properties to electrophysiological recording," *Sens. Actuators A, Phys.*, vol. 216, pp. 257–265, Sep. 2014.
- [21] G. Márton *et al.*, "The neural tissue around SU-8 implants: A quantitative *in vivo* biocompatibility study," *Mater. Sci. Eng., C*, vol. 112, Jul. 2020, Art. no. 110870.
- [22] B. J. Kim *et al.*, "3D Parylene sheath neural probe for chronic recordings," *J. Neural Eng.*, vol. 10, no. 4, Aug. 2013, Art. no. 045002.
- [23] J. W. Reddy, I. Kimukin, E. Towe, and M. Chamanzar, "Flexible, monolithic, high-density μ LED neural probes for simultaneous optogenetics stimulation and recording," in *Proc. 9th Int. IEEE/EMBS Conf. Neural Eng. (NER)*, Mar. 2019, pp. 831–834.
- [24] H. Xu, A. W. Hirschberg, K. Scholten, T. W. Berger, D. Song, and E. Meng, "Acute *in vivo* testing of a conformal polymer microelectrode array for multi-region hippocampal recordings," *J. Neural Eng.*, vol. 15, no. 1, Feb. 2018, Art. no. 016017.
- [25] T. Ware *et al.*, "Fabrication of responsive, softening neural interfaces," *Adv. Funct. Mater.*, vol. 22, no. 16, pp. 3470–3479, Aug. 2012.
- [26] A. Zátonyi *et al.*, "A softening laminar electrode for recording single unit activity from the rat hippocampus," *Sci. Rep.*, vol. 9, no. 1, p. 2321, Dec. 2019.
- [27] A. Stiller *et al.*, "Chronic intracortical recording and electrochemical stability of thiol-ene/acrylate shape memory polymer electrode arrays," *Micromachines*, vol. 9, no. 10, p. 500, Sep. 2018.
- [28] C. L. Kolarcik *et al.*, "Elastomeric and soft conducting microwires for implantable neural interfaces," *Soft Matter*, vol. 11, no. 24, pp. 4847–4861, 2015.
- [29] M. A. McClain, I. P. Clements, R. H. Shafer, R. V. Bellamkonda, M. C. LaPlaca, and M. G. Allen, "Highly-compliant, microcable neuroelectrodes fabricated from thin-film gold and PDMS," *Biomed. Microdevices*, vol. 13, no. 2, pp. 361–373, Apr. 2011.
- [30] J. P. Harris *et al.*, "In vivo deployment of mechanically adaptive nanocomposites for intracortical microelectrodes," *J. Neural Eng.*, vol. 8, no. 4, 2011, Art. no. 046010.
- [31] J. P. Harris *et al.*, "Mechanically adaptive intracortical implants improve the proximity of neuronal cell bodies," *J. Neural Eng.*, vol. 8, no. 6, Oct. 2011, Art. no. 066011.
- [32] S. P. Marshall, W.-C. Lin, P. R. Patel, A. J. Shih, and C. A. Chestek, "Effects of geometry and material on the insertion of very small neural electrode," in *Proc. 38th Annu. Int. Conf. IEEE Eng. Med. Biol. Soc. (EMBC)*, Aug. 2016, pp. 2784–2788.
- [33] A. Lecomte, E. Descamps, and C. Bergaud, "A review on mechanical considerations for chronically-implanted neural probes," *J. Neural Eng.*, vol. 15, no. 3, Jun. 2018, Art. no. 031001.
- [34] M. Jorfi, J. L. Skousen, C. Weder, and J. R. Capadona, "Progress towards biocompatible intracortical microelectrodes for neural interfacing applications," *J. Neural Eng.*, vol. 12, no. 1, Feb. 2015, Art. no. 011001.
- [35] M. A. Lebedev and M. A. L. Nicolelis, "Brain-machine interfaces: Past, present and future," *Trends Neurosci.*, vol. 29, no. 9, pp. 536–546, Sep. 2006.
- [36] W. M. Grill, S. E. Norman, and R. V. Bellamkonda, "Implanted neural interfaces: Biochallenges and engineered solutions," *Annu. Rev. Biomed. Eng.*, vol. 11, no. 1, pp. 1–24, Aug. 2009.
- [37] S. Felix *et al.*, "Removable silicon insertion stiffeners for neural probes using polyethylene glycol as a biodegradable adhesive," in *Proc. Annu. Int. Conf. IEEE Eng. Med. Biol. Soc.*, Aug. 2012, pp. 871–874.
- [38] T. D. Y. Kozai and D. R. Kipke, "Insertion shuttle with carboxyl terminated self-assembled monolayer coatings for implanting flexible polymer neural probes in the brain," *J. Neurosci. Methods*, vol. 184, no. 2, pp. 199–205, Nov. 2009.
- [39] Z. Zhao, X. Li, F. He, X. Wei, S. Lin, and C. Xie, "Parallel, minimally-invasive implantation of ultra-flexible neural electrode arrays," *J. Neural Eng.*, vol. 16, no. 3, Jun. 2019, Art. no. 035001.
- [40] J. Shi and Y. Fang, "Flexible and implantable microelectrodes for chronically stable neural interfaces," *Adv. Mater.*, vol. 31, no. 45, Nov. 2019, Art. no. 1804895.
- [41] J. E. Chung *et al.*, "Chronic implantation of multiple flexible polymer electrode arrays," *J. Visualized Exp.*, p. 152, Oct. 2019.
- [42] H. R. Joo *et al.*, "A microfabricated, 3D-sharpened silicon shuttle for insertion of flexible electrode arrays through dura mater into brain," *J. Neural Eng.*, vol. 16, no. 6, Oct. 2019, Art. no. 066021.
- [43] L. W. Tien, F. Wu, M. D. Tang-Schomer, E. Yoon, F. G. Omenetto, and D. L. Kaplan, "Silk as a multifunctional biomaterial substrate for reduced glial scarring around brain-penetrating electrodes," *Adv. Funct. Mater.*, vol. 23, no. 25, pp. 3185–3193, Jul. 2013.
- [44] C. Metallo and B. A. Trimmer, "Silk coating as a novel delivery system and reversible adhesive for stiffening and shaping flexible probes," *J. Biol. Methods*, vol. 2, no. 1, p. 13, Feb. 2015.
- [45] A. Lecomte *et al.*, "Silk and PEG as means to stiffen a Parylene probe for insertion in the brain: Toward a double time-scale tool for local drug delivery," *J. Micromech. Microeng.*, vol. 25, no. 12, Dec. 2015, Art. no. 125003.
- [46] T. Suzuki, K. Mabuchi, and S. Takeuchi, "A 3D flexible Parylene probe array for multichannel neural recording," in *Proc. 1st Int. IEEE EMBS Conf. Neural Eng., Conf.*, Mar. 2003, pp. 154–156.
- [47] K. J. Seo *et al.*, "Transparent, flexible, penetrating microelectrode arrays with capabilities of single-unit electrophysiology," *Adv. Biosyst.*, vol. 3, no. 3, 2019, Art. no. 1800276.
- [48] M.-C. Lo *et al.*, "Coating flexible probes with an ultra fast degrading polymer to aid in tissue insertion," *Biomed. Microdevices*, vol. 17, no. 2, p. 34, Apr. 2015.
- [49] D. Lewitus, K. L. Smith, W. Shain, and J. Kohn, "Ultrafast resorbing polymers for use as carriers for cortical neural probes," *Acta Biomaterialia*, vol. 7, no. 6, pp. 2483–2491, Jun. 2011.
- [50] J. Agorelius, F. Tsanakalis, A. Friberg, P. T. Thorbergsson, L. M. E. Pettersson, and J. Schouenborg, "An array of highly flexible electrodes with a tailored configuration locked by gelatin during implantation—initial evaluation in cortex cerebri of awake rats," *Frontiers Neurosci.*, vol. 9, p. 331, Sep. 2015.
- [51] G. Lind, C. E. Linsmeier, J. Thelin, and J. Schouenborg, "Gelatine-embedded electrodes—A novel biocompatible vehicle allowing implantation of highly flexible microelectrodes," *J. Neural Eng.*, vol. 7, no. 4, Aug. 2010, Art. no. 046005.
- [52] A. Singh, H. Zhu, and J. He, "Improving mechanical stiffness of coated benzocyclobutene (BCB) based neural implant," in *Proc. 26th Annu. Int. Conf. IEEE Eng. Med. Biol. Soc.*, Sep. 2004, pp. 4298–4301.
- [53] D. Kil *et al.*, "Dextran as a resorbable coating material for flexible neural probes," *Micromachines*, vol. 10, no. 1, p. 61, Jan. 2019.
- [54] Z. Xiang *et al.*, "Ultra-thin flexible polyimide neural probe embedded in a dissolvable maltose-coated microneedle," *J. Micromech. Microeng.*, vol. 24, no. 6, Jun. 2014, Art. no. 065015.
- [55] P. J. Gilgunn *et al.*, "An ultra-compliant, scalable neural probe with molded biodegradable delivery vehicle," in *Proc. IEEE 25th Int. Conf. Micro Electro Mech. Syst. (MEMS)*, Jan. 2012, pp. 56–59.
- [56] F. Pei and B. Tian, "Nanoelectronics for minimally invasive cellular recordings," *Adv. Funct. Mater.*, Dec. 2019, Art. no. 1906210.
- [57] V. Castagnola *et al.*, "Parylene-based flexible neural probes with PEDOT coated surface for brain stimulation and recording," *Biosensors Bioelectron.*, vol. 67, pp. 450–457, May 2015.
- [58] A. W. Hirschberg, H. Xu, K. Scholten, T. W. Berger, D. Song, and E. Meng, "Development of an anatomically conformal Parylene neural probe array for multi-region hippocampal recordings," in *Proc. IEEE 30th Int. Conf. Micro Electro Mech. Syst. (MEMS)*, Jan. 2017, pp. 129–132.
- [59] A. Weltman, H. Xu, K. Scholten, T. W. Berger, D. Song, and E. Meng, "Deep brain targeting strategy for bare Parylene neural probe arrays," in *Solid-State, Actuat., Microsyst. Workshop Tech. Dig.*, May 2016, pp. 302–305.

- [60] S. Yagi *et al.*, "Dissolvable base scaffolds allow tissue penetration of high-aspect-ratio flexible microneedles," *Adv. Healthcare Mater.*, vol. 4, no. 13, pp. 1949–1955, 2015.
- [61] B. A. Wester, R. H. Lee, and M. C. LaPlaca, "Development and characterization of *in vivo* flexible electrodes compatible with large tissue displacements," *J. Neural Eng.*, vol. 6, no. 2, Apr. 2009, Art. no. 024002.
- [62] W. Jensen, K. Yoshida, and U. G. Hofmann, "*In-vivo* implant mechanics of flexible, silicon-based ACREO microelectrode arrays in rat cerebral cortex," *IEEE Trans. Biomed. Eng.*, vol. 53, no. 5, pp. 934–940, May 2006.
- [63] C. S. Bjornsson *et al.*, "Effects of insertion conditions on tissue strain and vascular damage during neuroprosthetic device insertion," *J. Neural Eng.*, vol. 3, no. 3, pp. 196–207, Sep. 2006.
- [64] D. J. Edell, V. V. Toi, V. M. McNeil, and L. D. Clark, "Factors influencing the biocompatibility of insertable silicon microshafts in cerebral cortex," *IEEE Trans. Biomed. Eng.*, vol. 39, no. 6, pp. 635–643, Jun. 1992.
- [65] A. Sridharan, J. K. Nguyen, J. R. Capadona, and J. Muthuswamy, "Compliant intracortical implants reduce strains and strain rates in brain tissue *in vivo*," *J. Neural Eng.*, vol. 12, no. 3, Jun. 2015, Art. no. 036002.
- [66] K. Najafi and J. F. Hetke, "Strength characterization of silicon microprobes in neurophysiological tissues," *IEEE Trans. Biomed. Eng.*, vol. 37, no. 5, pp. 474–481, May 1990.
- [67] S. Singh *et al.*, "Modeling the insertion mechanics of flexible neural probes coated with sacrificial polymers for optimizing probe design," *Sensors*, vol. 16, no. 3, p. 330, Mar. 2016.
- [68] E. Meng, P.-Y. Li, and Y.-C. Tai, "Plasma removal of Parylene C," *J. Micromech. Microeng.*, vol. 18, no. 4, Apr. 2008, Art. no. 045004.
- [69] S. Dabral *et al.*, "Stress in thermally annealed Parylene films," *J. Electron. Mater.*, vol. 21, no. 10, pp. 989–994, Oct. 1992.
- [70] J. Ortigoza-Diaz, K. Scholten, and E. Meng, "Characterization and modification of adhesion in dry and wet environments in thin-film Parylene systems," *J. Microelectromech. Syst.*, vol. 27, no. 5, pp. 874–885, Oct. 2018.
- [71] H. M. Gensler and E. Meng, "Rapid fabrication and characterization of MEMS Parylene C bellows for large deflection applications," *J. Micromech. Microeng.*, vol. 22, no. 11, Nov. 2012, Art. no. 115031.
- [72] A. A. Sharp, A. M. Ortega, D. Restrepo, D. Curran-Everett, and K. Gall, "*In vivo* Penetration mechanics and mechanical properties of mouse brain tissue at micrometer scales," *IEEE Trans. Biomed. Eng.*, vol. 56, no. 1, pp. 45–53, Jan. 2009.
- [73] N. A. Alcantar, E. S. Aydil, and J. N. Israelachvili, "Polyethylene glycol-coated biocompatible surfaces," *J. Biomed. Mater. Res.*, vol. 51, no. 3, pp. 343–351, 2000.
- [74] Z.-J. Chen *et al.*, "A realistic brain tissue phantom for intraparenchymal infusion studies," *J. Neurosurgery*, vol. 101, no. 2, pp. 314–322, Aug. 2004.
- [75] A. Andrei, M. Welkenhuysen, B. Nuttin, and W. Eberle, "A response surface model predicting the *in vivo* insertion behavior of micromachined neural implants," *J. Neural Eng.*, vol. 9, no. 1, Feb. 2012, Art. no. 016005.
- [76] S. A. Hara, B. J. Kim, J. T. W. Kuo, and E. Meng, "An electrochemical investigation of the impact of microfabrication techniques on polymer-based microelectrode neural interfaces," *J. Microelectromech. Syst.*, vol. 24, no. 4, pp. 801–809, Aug. 2015.
- [77] N. A. B. Ismail, F. Abd-Wahab, and W. W. A. W. Salim, "Cyclic voltammetry and electrochemical impedance spectroscopy of partially reduced graphene oxide—PEDOT:PSS transducer for biochemical sensing," in *Proc. IEEE-EMBS Conf. Biomed. Eng. Sci. (IECBES)*, Dec. 2018, pp. 330–335.
- [78] J. M. Hsu, S. Kammer, E. Jung, L. Rieth, R. A. Normann, and F. Solzbacher, "Characterization of Parylene-C film as an encapsulation material for neural interface devices," in *Proc. Conf. Multi-Mater. Micro Manuf.*, 2007, pp. 1–4.
- [79] S. F. Cogan, "Neural stimulation and recording electrodes," *Annu. Rev. Biomed. Eng.*, vol. 10, no. 1, pp. 275–309, Aug. 2008.
- [80] H. Xu, A. W. Hirschberg, K. Scholten, E. Meng, T. W. Berger, and D. Song, "Application of Parylene-based flexible multi-electrode array for recording from subcortical brain regions from behaving rats," in *Proc. 40th Annu. Int. Conf. IEEE Eng. Med. Biol. Soc. (EMBC)*, Jul. 2018, pp. 4599–4602.
- [81] M. Welkenhuysen, A. Andrei, L. Ameye, W. Eberle, and B. Nuttin, "Effect of insertion speed on tissue response and insertion mechanics of a chronically implanted silicon-based neural probe," *IEEE Trans. Biomed. Eng.*, vol. 58, no. 11, pp. 3250–3259, Nov. 2011.
- [82] J. A. Thornton and D. W. Hoffman, "Stress-related effects in thin films," *Thin Solid Films*, vol. 171, no. 1, pp. 5–31, Apr. 1989.
- [83] T. Noguchi, "Effect of thermal annealing on sputtered a-Si film," *J. Korean Phys. Soc.*, vol. 45, pp. S847–S850, Dec. 2004.



Xuechun Wang (Student Member, IEEE) received the B.S. degree from the Biomedical Engineering Department, Joint Department of UNC Chapel Hill and NC State University, in 2017. She is currently pursuing the Ph.D. degree in biomedical engineering with the Biomedical Microsystems Laboratory, University of Southern California. Her current research interest includes flexible neural interface and sensor design. She was a recipient of the USC Provost's Diversity, Inclusion, and Access (DIA) Fellowship and ARCS scholar reward.



Ahuva Weltman Hirschberg received the B.S. degree in bioengineering from the University of California, Los Angeles, in 2012, and the Ph.D. degree in biomedical engineering from the University of Southern California, in 2018, with a focus on flexible and penetrating neural implants, under the supervision of Dr. E. Meng. She is currently pursuing the degree in medical with the Keck School of Medicine, University of Southern California.



Huijing Xu (Member, IEEE) received the B.S. degree in biomedical engineering from Shanghai Jiao Tong University and the Ph.D. degree in biomedical engineering from the University of Southern California in 2019. After her B.S., she continued studying in this field at USC and developed her interests in neural engineering and cortical prostheses. In 2011, she joined the Center for Neural Engineering (CNE), where she is currently working under the direction of Prof. T. W. Berger and Prof. D. Song. Her research focuses on the development of novel neural interfacing techniques and the understanding of the function of the hippocampus in memory processing. In specific, she also works on the design and development of conformal multi-electrode arrays that can record neural activities from multiple sub-regions of the hippocampus simultaneously from behaving animals and to conduct behavioral experiments to study the information transformation within the hippocampus tri-synaptic circuit.



Zachary Slingsby-Smith received the M.Eng. degree in material science and engineering from Imperial College London in 2016, where he is currently pursuing the Ph.D. degree in electrical engineering with the Optical and Semiconductors Laboratory.



Aziliz Lecomte received the M.D. degree in physics engineering from the INSA Engineering School, Toulouse, France, in 2013, and the Ph.D. degree from the LAAS-CNRS Lab in 2016. She worked on flexible polymer-based neural probes for chronic implantation with the LAAS-CNRS Lab. In 2015, she was a Visiting Scholar with the University of Southern California, in the team of Dr. E. Meng. In 2016, she received the l'Oréal-Unesco Grant For Women in Science. She is currently a Post-Doctoral Researcher with the Italian Institute of Technology (IIT), Genoa, Italy, with Dr. L. Berdondini, where she also works on CMOS-based high-density implantable neural probes.



Dong Song (Senior Member, IEEE) received the B.S. degree in biophysics from the University of Science and Technology of China in 1994, and the Ph.D. degree in biomedical engineering from the University of Southern California in 2004. He became a Research Assistant Professor and a Research Associate Professor with the Department of Biomedical Engineering, USC, in 2006 and 2013, respectively. He is currently the Co-Director of the Center for Neural Engineering, USC. His research interests include nonlinear dynamical modeling of the nervous system, hippocampal memory prosthesis, neural interface technologies, and development of novel modeling strategies incorporating both statistical and mechanistic modeling methods. He received the James H. Zumberge Individual Award at USC in 2008, the Outstanding Paper Award of IEEE TRANSACTIONS ON NEURAL SYSTEMS AND REHABILITATION ENGINEERING in 2013, and the Society for Brain Mapping and Therapeutics Young Investigator Award in 2018. He is a member of American Statistical Association, Biomedical Engineering Society, IEEE, Society for Neuroscience, Society for Brain Mapping and Therapeutics, Organization for Computational Neurosciences, and National Academy of Inventors. His research is supported by DARPA, NSF, and NIH.



Kee Scholten (Member, IEEE) received the B.S. degree in applied physics from the California Institute of Technology in 2009 and the Ph.D. degree from the University of Michigan in 2014 with Prof. E. Zellers. He completed his Postdoctoral studies with the Biomedical Microsystems Laboratory, University of Southern California, in 2019, with Prof. E. Meng, where he is currently the Director of the Polymer Implantable Electrode Foundry. His research explores the development of micro- and nano-technology for ubiquitous chemical and biomedical sensing, with a focus on polymer-based MEMS and flexible electronics.



Ellis Meng (Fellow, IEEE) received the B.S. degree in engineering and applied science and the M.S. and Ph.D. degrees in electrical engineering from the California Institute of Technology (Caltech), Pasadena, in 1997, 1998, and 2003, respectively. Since 2004, she has been with the University of Southern California, Los Angeles, where she was the Viterbi Early Career Chair and then the Department Chair. She is currently Professor of biomedical engineering and holds a joint appointment with the Ming Hsieh Department of Electrical and Computer Engineering. She also serves as the Vice Dean for Technology Innovation and Entrepreneurship. Her research interests include bioMEMS, implantable biomedical microdevices, microfluidics, multimodality integrated microsystems, and packaging. She is a fellow of ASME, BMES, AIMBE, and NAI. She was a recipient of the Intel Women in Science and Engineering Scholarship, the Caltech Alumni Association Donald S. Clark Award, and the Caltech Special Institute Fellowship. She has also received the NSF CAREER and Wallace H. Coulter Foundation Early Career Translational Research Awards. In 2009, she was recognized as one of the TR35 Technology Review Young Innovators under 35.